Published in IET Generation, Transmission & Distribution
Received on 25th June 2011
Revised on 15th October 2011
doi: 10.1049/iet-gtd.2011.0476

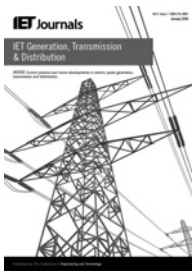

ISSN 1751-8687

Development of a new derivative-based algorithm to detect current transformer saturation

A. Hooshyar M. Sanaye-Pasand M. Davarpanah

Control and Intelligent Processing Center of Excellence, School of Electrical and Computer Engineering, College of Engineering, University of Tehran, Iran
E-mail: alihooshyar@gmail.com

Abstract: Derivative-based approaches have been used both in the literature and in the industry to identify fault current distortions caused by current transformer (CT) saturation. This study presents a new simple, but efficient, derivative-based technique to detect CT saturation. First a difference function for the samples on the two sides of the current local extremum is defined. Based on the values of this difference function for various current samples, a variance function is defined. By comparing this variance function with a pair of pre-set thresholds, CT saturation can be determined. This technique is not affected by CT parameters such as CT burden, core remanence or magnetisation curve. The independence of this method from the fault current characteristics, such as decaying DC time constant, noise and so on, is investigated. Numerous simulations were carried out using PSCAD/EMTDC program. The performance of this algorithm for simulated fault currents together with a set of experimental results verify the accurate operation of the proposed method for different conditions including mild and fast CT saturations.

1 Introduction

The current flowing in a power system rises significantly after occurrence of a short-circuit fault. Current transformers (CTs) should supply the protective relays by stepping down the level of this current, while preserving its original waveshape. If the fault current is a perfect sinusoid, the appropriately designed CTs maintain a high accuracy, even if the current amplitude is very high. However, fault currents often contain an appreciable amount of decaying DC component. This component generates an extra DC flux in the CT iron core and may cause CT saturation. The current reproduced by a saturated CT may be considerably different from the real fault current in the power circuit. Therefore it can lead to maloperation of the protective relays [1].

In industrial applications, some protective relays detect CT saturation based on the harmonic content of the current waveform [2]. However, this method requires one full cycle to provide a reliable response. Some of the differential relays identify CT saturation during external faults using the relation between variation rates of the differential and restraining quantities [3]. This method can be used only to detect saturation during external faults for differential relays. Another way to tackle the CT saturation problem is the alternative use of Rogowski coil instead of iron-core CTs for the relaying purposes [4, 5]. However, iron-core CTs have been widely used and still are being installed in almost all of the power systems around the world and protection engineers are inevitably confronted with the problem of CT saturation.

Recently different methods have been proposed to detect CT saturation [6–18]. In [6] the zero-sequence differential current gradient with respect to the bias current is calculated to identify the saturation. This method is confined to differential relays. Artificial neural networks (ANN) have been used in [7] to detect and compensate for CT saturation. ANN-based methods may require considerable amount of data to be trained properly.

Many CT saturation detection techniques are based on the waveshape properties of distorted fault currents. Mathematical morphology is used to determine the non-smooth changes at the beginning and the end of a distorted fault current in [8, 9]. Wavelet transform has been employed in [10, 11] to identify CT saturation by analysing the high-frequency content of current waveform. Hence, these methods can be noise sensitive.

Some of the recent CT saturation detection methods employ digital filtering algorithms. The decaying DC component of fault current measured by phasor-based computations is exploited to define a saturation detection index in [12]. Using least error squares technique, distorted and undistorted sections of current inside a symmetrical variable-length window are compared to each other to detect CT saturation in [13].

The derivatives of current waveform are introduced in [14] to detect CT saturation. It is shown that during non-saturated conditions, the third derivative of current remains below a threshold specified by the expected maximum fault current. This technique was then used in several saturation compensation methods for detecting the instant of saturation [15, 16]. The main drawback of this method is that the threshold setting criterion is system dependent. The selected threshold must be adjusted regularly based on the short-circuit capacity of the system.

Some other derivative-based saturation detection techniques have been published recently. In [17] CT saturation can be identified correctly, unless the fault current is contaminated with harmonics or noise. One of the techniques proposed in [18] compares the current second derivative with an adaptive threshold, which is not system dependent. This algorithm might not be able to detect all fast and mild CT saturations reliably. Derivative-based techniques have also been accepted and used by some relay manufacturers as effective ways to detect CT saturation [19].

This paper proposes a new simple, yet efficient and reliable derivative-based technique to identify CT saturation. This method is not affected by noise and fault current characteristics such as decaying DC time constant. It is also independent of the CT parameters, such as its burden and remanence. Extensive numbers of simulations confirm the fast and reliable performance of the proposed method. The advantages of this method over the other adaptive and non-adaptive derivative-based saturation detection techniques have also been discussed throughout the paper.

2 Proposed features for current derivatives

2.1 DC-offset-free fault currents

In the first step, it is assumed that the fault current does not include a decaying DC component and is purely sinusoidal. As an example, consider the discrete current signal described by (1)

$$\mathrm{i}[n] = \sin\left[2\pi 50(n\Delta T) - \frac{\pi}{2}\right] \tag{1}$$

ΔT is the sampling period which is 0.4 ms in this paper. Consider a window which begins after the current zero-crossing and the current extremum is sited at its centre. In other words, if the sampling instants just after the current zero-crossing and at the current extremum are denoted by n_o and n_m, respectively, this window contains $i[n]$ samples for $n_o < n < 2\,n_m - n_o$. This window for the $i[n]$ described by (1) is shown in Fig. 1*a*. It can be seen that the samples inside this window are symmetrical with respect to the vertical line which passes through n_m.

The first difference function [20] of current waveform inside the defined window is denoted by d_1. d_1 for the current $i[n]$ defined by (1) is shown in Fig. 1*b*. This figure illustrates that owing to the symmetry of the sinusoidal waveform, d_1 has the same value, but with opposite signs, in the first and the second halves of its domain; that is, before and after n_m. The first variance function defined by (2) measures the degree of similarity between the two halves of d_1

$$\delta_1[n_m + n] = \left[\frac{d_1[n_m + n] + d_1[n_m - n]}{i_m}\right] \times 100 \tag{2}$$

in which i_m is the value (including sign) of the current extremum at n_m. The domain of the first variance function is $[n_m + 1,\ 2n_m - n_o]$. For purely sinusoidal currents, δ_1 is always zero.

The second difference function inside the above-discussed window is denoted by d_2. As shown in Fig. 1*c*, if a signal is sinusoidal, the two halves of d_2 inside the window will have the same sign and magnitude. Similar to δ_1, the second variance function is defined to measure the degree of similarity between the two halves of d_2

$$\delta_2[n_m + n] = \left[\frac{d_2[n_m + n] - d_2[n_m - n]}{i_m}\right] \times 100 \tag{3}$$

The domain of the second variance function is $[n_m + 2,\ 2n_m - n_o]$. The symmetry of a sinusoidal current leads to zero value for δ_2, as well.

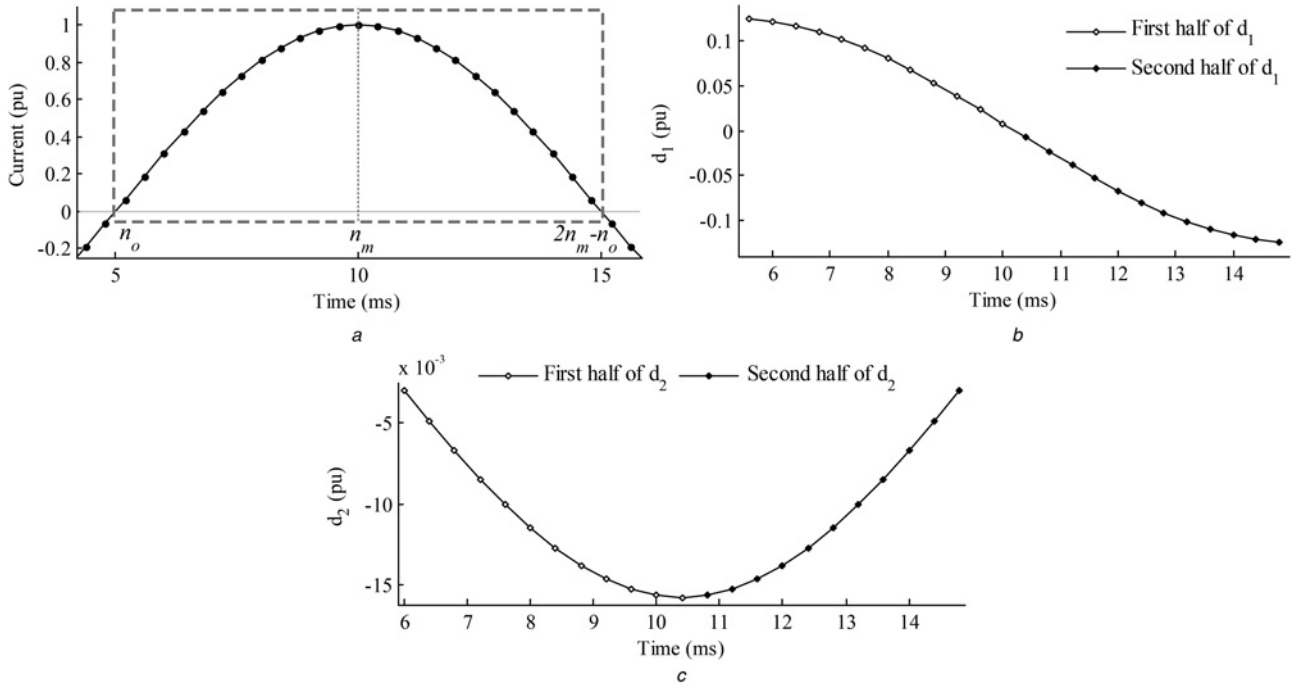

Fig. 1 *Analysis of the DC-offset-free current defined by (1)*

a Current signal
b First difference function
c Second difference function

doi: 10.1049/iet-gtd.2011.0476

2.2 Fault currents including decaying DC-offset

Apart from the fundamental frequency component, the fault current often includes a decaying DC-offset. As an example, consider $i[n]$ described by (4)

$$i[n] = \sin\left[2\pi 50(n\Delta T) - \sin^{-1}(I_{\mathrm{d}})\right] + I_{\mathrm{d}} \exp\left[\frac{-n\Delta T}{\tau}\right] \quad (4)$$

in which I_{d} and τ are the initial magnitude and time constant of the decaying DC component. This signal for $I_{\mathrm{d}} = 1$ and $\tau = 30$ ms, has been plotted in Fig. 2*a*.

In the presence of the decaying DC component, the symmetry of current waveform with respect to n_m inside the defined window is very slightly affected. As shown in Figs. 2*b* and *c*, the first and the second halves of difference functions are not exactly identical anymore; however, they are still very similar. Hence, the two variance functions take non-zero, but tiny, values. This is illustrated for the i[n] described by (4) in Fig. 2*d*. It is observed that the values of δ_1 and particularly δ_2 remain very small. The maximum and the minimum of δ_1 are 0.70 and −2.04%, respectively. δ_2 is negative during the whole span of the window and its minimum is only −0.23%.

In order to obtain the maximum and the minimum values of the variance functions for all of the possible undistorted fault currents, I_{d} and τ of (4) were varied in the ranges of $0 \leq I_{\mathrm{d}} \leq 1$ and $0.5 \leq \tau \leq 5$ cycles. For each case, the lowest and the highest values of δ_1 and δ_2 were measured. The obtained results indicate that the first and the second variance functions for undistorted fault currents are confined to the ranges of $-6.13\% \leq \delta_1 \leq 1.58\%$ and $-0.47\% \leq \delta_2 \leq 0.16\%$, respectively. In other words, the two variance functions, specially the second variance function, are very small when the fault current is not affected by CT saturation.

It should be mentioned that the above variance functions limits hold true for the negative DC-offset value as well, since i_m in the denominator of (2) and (3) includes the sign of current extremum.

2.3 Fault currents distorted by CT saturation

When the CT saturates after the onset of a fault, the derivatives of current will change significantly [14, 18]. As will be shown later on, for most of the saturation cases, CT saturation begins at or after the secondary current local extremum (n_m). In other words, only the second half of the current window is affected by CT saturation. Therefore the values of the difference functions in the two halves of the window will be widely different. In the performance evaluation section, it will be shown that even for the rare cases in which the CT saturation begins before the secondary current extremum, the difference functions have very different magnitudes at the two sides of n_m inside the window. Different values of d_1 and d_2 at the two sides of n_m lead to substantial increase in δ_1 and δ_2 for most of the samples during the saturated period.

Fig. 3*a* depicts the primary and secondary currents of a saturated CT during the first cycle after the inception of a fault at $t = 200$ ms. The CT saturation depicted in this figure begins after the primary current extremum. In such conditions, the extremum of the secondary current is the same as that of the primary current. As a result, the distorted part of current begins after n_m and, as mentioned above, only the second half of the window is affected by CT saturation. The CT is saturated at $t = 212.8$ ms, that is, seven samples after n_m. It is shown that during the few milliseconds after the beginning of the saturation, the secondary current begins

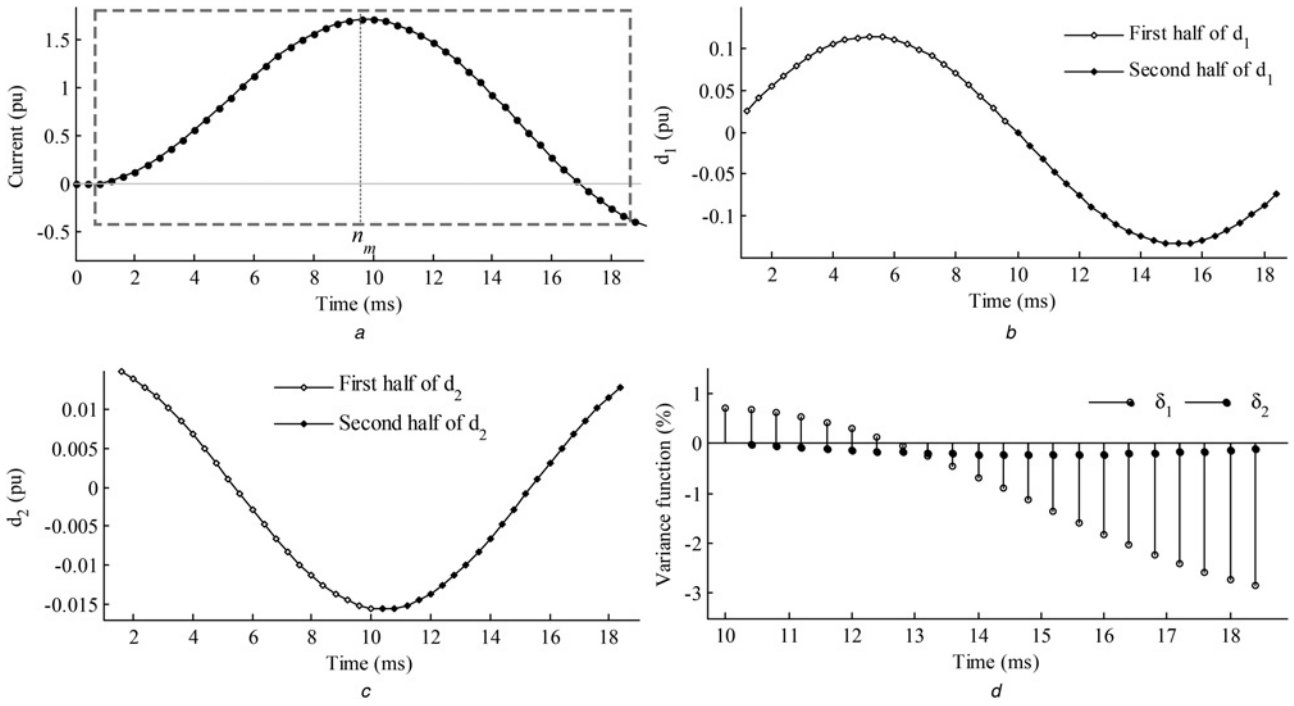

Fig. 2 *Analysis of a typical fault current including decaying DC-offset*

a Current signal defined by (4)
b First difference function
c Second difference function
d First and the second variance functions

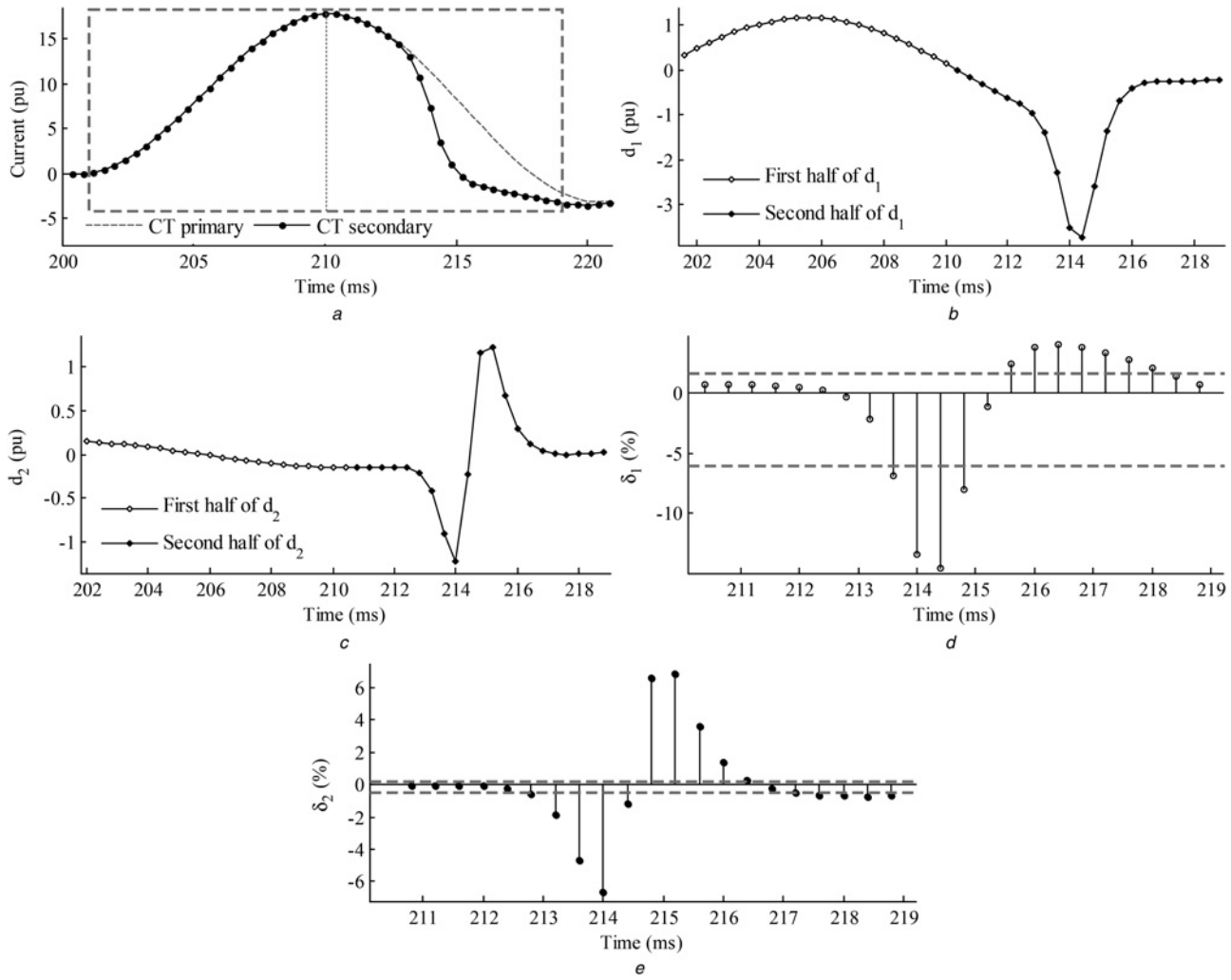

Fig. 3 *Analysis of a fault current distorted by CT saturation*

a Fault current
b First difference function
c Second difference function
d First variance function
e Second variance function

to decline sharply. In this period, magnitude of the current gradient is substantially larger than that before n_m. After this initial period, slope of the secondary current decreases considerably. Therefore at the end of the distorted section, the gradient is smaller than that before n_m. The difference between the current gradients magnitudes before and after n_m is well observed in Fig. 3*b*. In addition, Fig. 3*c* shows that a similar scenario applies for the second difference function d_2. Immediately after the saturation, d_2 has a large negative value. Then, it increases to a large positive value. As a result, the values and the pattern of d_2 during the two halves of the window are widely different.

Different values of the difference functions before and after the current extremum are directly reflected in the variance functions. The first variance function for the CT secondary current is shown in Fig. 3*d*. In this figure, the dashed horizontal lines represent the limits of δ_1 obtained for undistorted fault currents as presented in the previous subsection. It is shown that δ_1 exceeds the horizontal line at $t = 213.6$ ms, that is, two samples after beginning of the saturation. The distance between δ_1 and the limit line increases for the subsequent samples. At $t = 214.4$ ms, δ_1 is about 2.5 times larger than the lower limit.

Fig. 3*e* depicts the second variance function δ_2 for the CT secondary current. The dashed horizontal lines are the limits of δ_2 obtained for undistorted fault currents. It is shown that the value of δ_2 is about the lower limit as soon as the CT saturates. After only one sample, the magnitude of δ_2 is about four times larger than the lower limit. The difference between the second variance function and the limit line reaches its maximum at $t = 215.2$ ms, when δ_2 is more than 40 times larger than the upper limit.

3 Proposed decision-making algorithm

Figs. 3*d* and *e* suggest that by using a simple fixed thresholding scheme, the defined variance functions could reliably identify CT saturation. Comparing Figs. 3*c* and *d*, it is found that the CT saturation can be detected faster and also more reliably using the second variance function δ_2. Therefore application of δ_2 is proposed for detecting CT saturation. The threshold setting criterion is based on the upper and lower limits of δ_2 obtained for undistorted fault currents. In order to compensate for the probable effects of noise, relatively large security margins are added to these limits to determine the final thresholds. These security

doi: 10.1049/iet-gtd.2011.0476

margins have to guarantee the dependability of the proposed method for mild CT saturations and its security for noisy undistorted fault currents. The selected security margins for the lower and upper thresholds are 200 and 400%, respectively; that is, −1.40 and 0.82% are set as the lower and upper thresholds of δ_2. A larger security margin is considered for the upper threshold, as the upper limit of δ_2 for undistorted fault currents has a smaller value and, thus, it might be more vulnerable to noise. In addition, in later sections it will be shown that the second variance function is beyond the above thresholds during mild CT saturations.

The proposed method is initiated as soon as a pick-up signal is issued by a simple fault detector unit, which can determine the occurrence of a disturbance by using only a few current samples [21]. Then the window described in the previous section is placed on the fault current after each odd zero-crossing. When the extremum of current inside the window is passed, the second variance function is evaluated. If δ_2 exceeds the specified thresholds for two consecutive samples, CT saturation is detected; otherwise, the CT is not saturated. Fig. 4 shows the flowchart of the proposed algorithm.

Unlike the previous derivative-based CT saturation detection techniques, this method does not compare the current derivatives (difference functions) with fixed or adaptive thresholds. Instead, the derivatives of current waveform at the two sides of its local extremum are subtracted from each other, and then the result is compared with a pair of preset fixed thresholds. One of the advantages of this approach over some other derivative-based saturation detection techniques such as [14] is that the employed pair of thresholds is not system dependent. In other words, there is no need to adjust the thresholds based on the power system parameters and conditions.

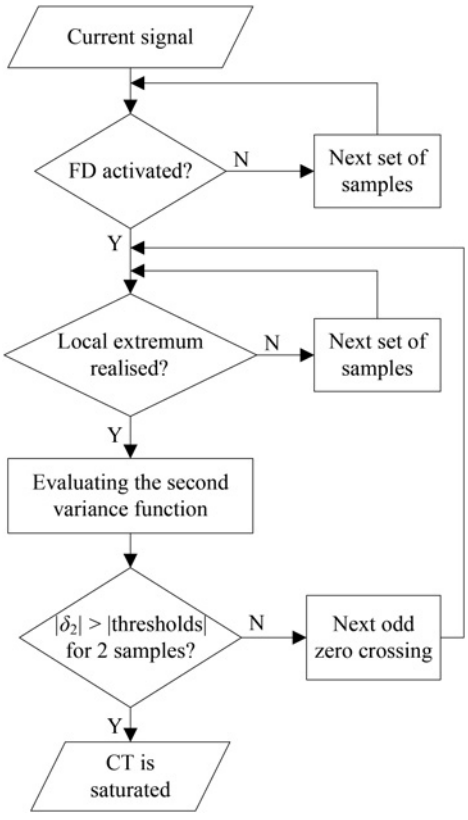

Fig. 4 *Flowchart of the proposed method*

Another drawback of some derivative-based techniques emerges when the CT is saturated mainly because of large CT remanence, whereas the fault current magnitude is relatively small. Since the fault current is small and the threshold is based on the maximum possible fault current [14], the difference function can be smaller than the threshold in such conditions. Meanwhile, the performance of the proposed method is not dependent on the fault current magnitude, as the current derivatives are divided by i_m in (3). So, the proposed technique can reliably detect CT saturation irrespective of the fault current magnitude.

4 Performance evaluation

In order to test the performance of the proposed method, the power system described in the appendix was simulated using the PSCAD/EMTDC software. The operation of the proposed method for analysing the CTs used for protection of busbar B_5 was thoroughly examined. These CTs were dimensioned based on half of the minimum CT requirements of a modern and widely used relay [22]. Owing to this sizing criterion, the simulated CTs were saturated faster and more severely.

Numerous simulations were carried out and encouraging results were obtained. In the simulations, various parameters which affect the transient response of a CT, such as magnitude and power factor of the CT burden, fault inception angle, time constant of the power system, fault resistance and so on, were changed. CT saturation was simulated using the Lucas [23] and Jiles-Atherton [24] CT models and similar successful results were achieved for both of these models. Different magnetisation curves, including the Silectron 53, which is available in PSCAD, were considered in the simulations. Depending on the class of a CT, its remanence may reach up to 90% of the saturation flux [25]. The actual remanence of a closed iron core CT can be even larger after an unsuccessful auto-reclosing [26]. Therefore different amounts of residual flux in the range of −95% to +95 were applied. In this section, some of the obtained results are presented.

4.1 Case studies

4.1.1 Fast CT saturation: Unlike the case discussed in Fig. 3, for a fast CT saturation, the saturation is generally deeper and it begins before the primary current extremum. As a result, the local extremum of CT secondary current is located before the extremum of primary current. In such a condition, the variation pattern of the variance function is different from the one depicted in Fig. 3*e*. Fig. 5*a* depicts the current passing through the line L_{15} CT for a three-phase fault on this line adjacent to the busbar B_5 at $t = 199.6$ ms. The CT remanence is 70% and it is severely saturated at $t = 205.2$ ms, about a quarter-cycle after onset of the fault. Unlike Fig. 3*a*, here the saturation begins before the primary current extremum. In such conditions, the current drops down after the beginning of saturation. Therefore the instant of saturation inception becomes the secondary current extremum, n_m. Hence, only the second part of the window that begins after n_m, are affected by CT saturation.

The second difference function inside the window under study is plotted in Fig. 5*b*. As shown, the values of d_2 at the two sides of n_m differ considerably. As a result, the magnitude of the second variance function shown in Fig. 5*c* is very large. The main feature of the variance function during fast CT saturations is that it can detect saturation as

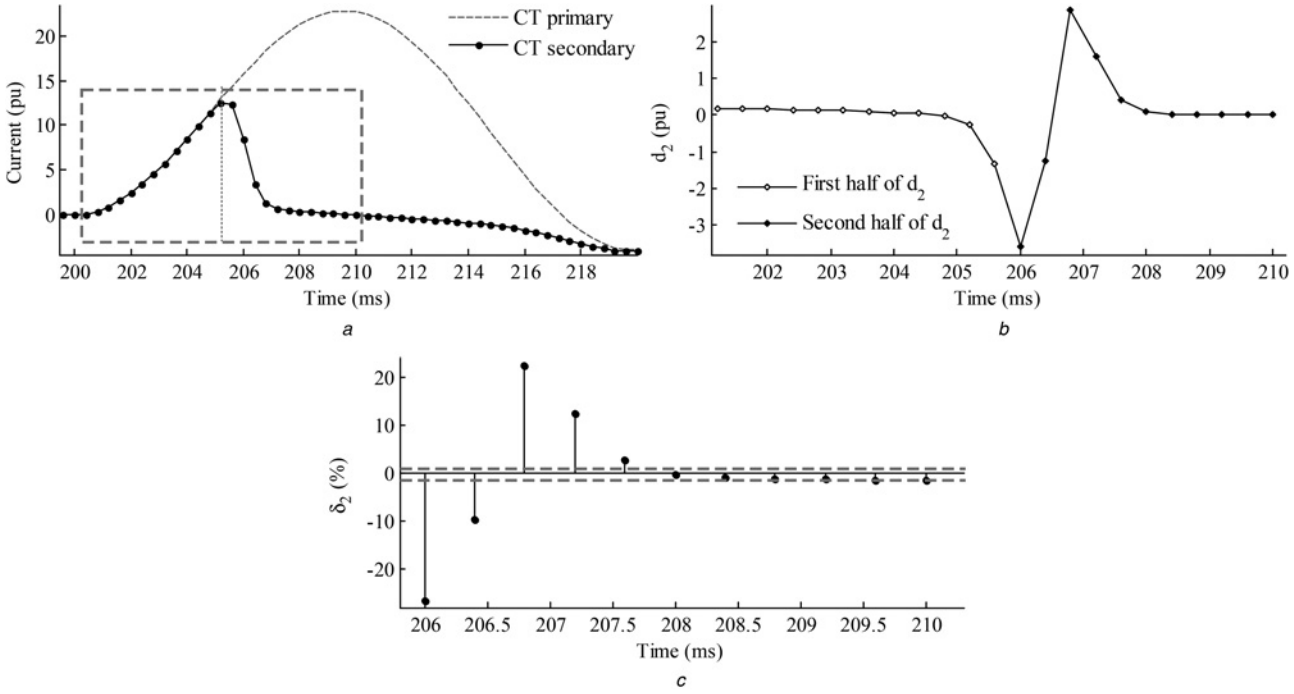

Fig. 5 *Fast CT saturation*

a CT primary and secondary currents
b Second difference function
c Second variance function

soon as the proposed method is initiated. Saturation is detected at $t = 206.4$ ms, when δ_2 exceeds the lower threshold for two consecutive samples. The large difference between δ_2 and its thresholds demonstrate the reliability of the proposed method. The largest difference between the second variance function and its thresholds occurs at $t = 206.8$ ms when δ_2 is more than 27 times larger than the upper threshold.

As shown by this example, one of the advantages of the proposed technique over the adaptive derivative-based technique of [18] is its ability to promptly detect fast CT saturations.

4.1.2 Very fast CT saturation: In this paper, CT saturations which occur in less than 3 ms after the fault inception are designated as very fast CT saturations. Very fast CT saturation is rarely observed in power systems owing to appropriate selection of CTs, that is, considering the CT requirements for protective relays. For differential relays, these requirements must guarantee a minimum saturation-free time, so that:

1. The relay measures the internal fault currents correctly.
2. The relay does not maloperate during external faults.

In the case of busbar differential relays, the external fault currents are generally larger than the internal fault currents because of the in-feed effect. Therefore the relay CT requirements are determined based on the condition 2 mentioned above. If very fast CT saturations during external faults could be detected by the relay saturation detector unit, the relay CT requirements can just be based on the condition 1. This new CT requirements impose a smaller CT core size because of the lower magnitude of internal fault currents.

Fig. 6*a* shows the current of the CT installed on line L_{56} for a three-phase fault on this line adjacent to the busbar B_5 at $t = 199.5$ ms. The CT remanence is 95%. Fig. 6*b* zooms in on the first half-cycle of the fault current. As shown, the CT secondary current begins to deviate from the primary current in less than 2 ms after the fault inception. This time is lower than the saturation-free time required by many industrial relays. As a result of the severe and very fast CT saturation, the saturation begins before the secondary current extremum (n_m); that is, both halves of the current inside the window shown in Fig. 6*b* are affected by saturation. Nonetheless, there still exists a great difference between the current derivatives at these two halves of the window. This can be seen in Fig. 6*c*, where the second variance function has been plotted. Here again, there is a reliable margin between δ_2 and the specified thresholds. Saturation is detected at $t = 204.0$ ms when δ_2 is larger than its thresholds for two successive samples. At this time, δ_2 is more than 12 times larger than its threshold.

Several other cases of very fast CT saturations were also simulated and examined. Some of the obtained results are presented in Table 1. In this table $\delta_{2,1}$ and $\delta_{2,2}$ are the values of δ_2 for the two successive samples by which saturation is detected. Δt_{SD} is the difference between the saturation inception and saturation detection times. The displayed results verify that the proposed method responds accurately, no matter how fast the CT saturates. Therefore if the proposed method is incorporated into a busbar differential relay, the CT could be dimensioned just to meet only condition 1 mentioned above.

4.1.3 Mild CT saturation: The proposed technique is highly sensitive to distortions caused by CT saturation and can detect very mild saturations. Fig. 7*a* shows the current of line L_{35} for a double-phase-to-ground fault on this line near the busbar B_5 at $t = 200$ ms. The level of saturation is very low and the measured secondary current slightly deviates from the CT primary current at $t = 215.2$ ms. The

doi: 10.1049/iet-gtd.2011.0476

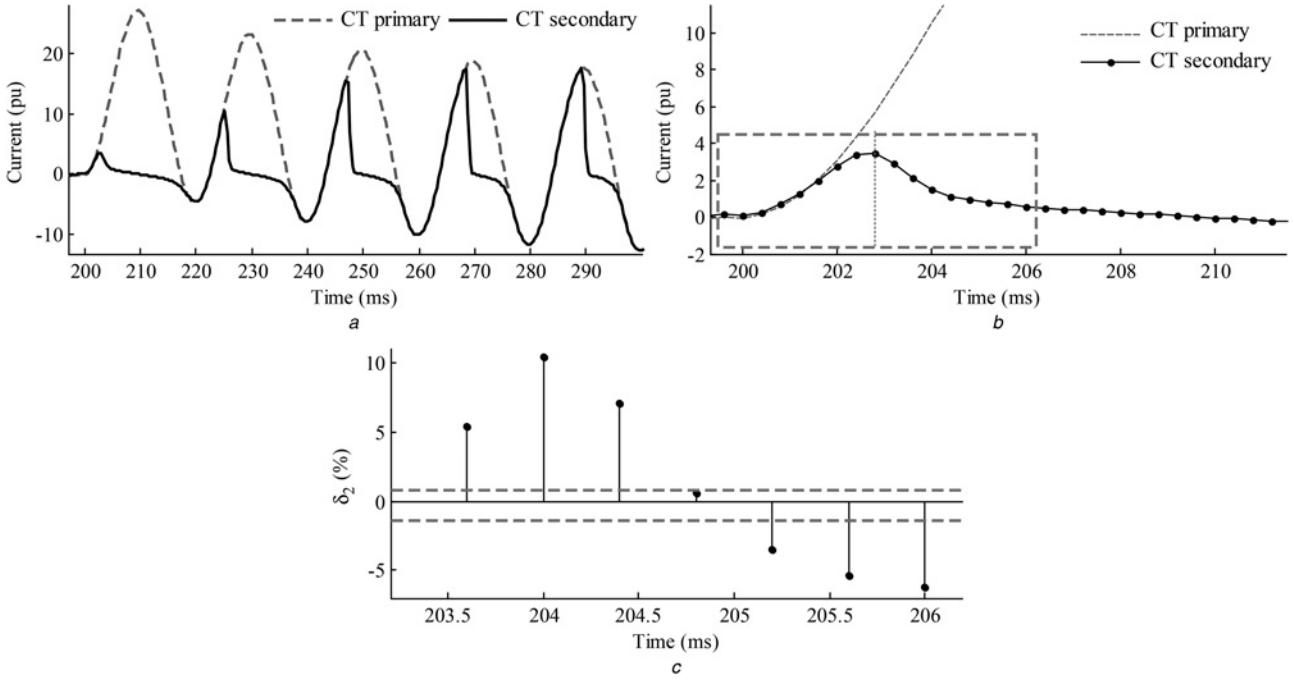

Fig. 6 *Very fast CT saturation*

a CT primary and secondary currents
b CT current in the first half-cycle after the fault
c Second variance function

Table 1 Obtained results for very fast CT saturation events

Fault type	Fault location	φ_r, %	Δt_{SD}, ms	$\delta_{2,1}$, %	$\delta_{2,2}$, %
ABG	L_{45}	95	2.0	4.3	14.7
ABCG	L_{45}	85	2.0	−6.9	17.6
ABCG	L_{45}	90	2.4	−3.2	15.5
ABCG	L_{45}	95	2.4	4.0	14.1
ABG	L_{15}	95	1.6	−7.5	17.4
ABCG	L_{15}	85	1.2	−9.9	16.1
ABCG	L_{15}	90	1.6	−7.3	18.3
ABCG	L_{15}	95	2.0	−4.4	16.9
ABG	L_{56}	95	2.0	4.7	11.6
ABCG	L_{56}	85	2.0	−3.1	16.0
ABCG	L_{56}	90	2.4	3.6	12.5
ABCG	L_{56}	95	2.4	6.0	10.3

saturation level is so low that the zero crossings of the primary and secondary currents at the end of the first cycle are only 1 ms apart. Despite the low degree of saturation, Fig. 7*b* depicts that the second variance function can still determine saturation quickly. CT saturation is detected at $t = 216.8$ when δ_2 exceeds its threshold for two consecutive samples. At this time, δ_2 is 1.76 times larger than its upper threshold.

The ability to detect mild CT saturations is another advantage of the proposed technique over the previous adaptive derivative-based methods. Fig. 7*c* shows the magnitude of the second derivative of fault current together with the adaptive threshold suggested in [18]. The security margin considered for the adaptive threshold in Fig. 7*c* is 60%, which is quite smaller than the 200 and 400% security margins used in this paper. Owing to the initial non-accurate estimation of the adaptive threshold in Fig. 7*c*, the current second derivative is higher than its threshold in the initial fraction of a cycle after the fault, although the CT is not saturated in that section. On the other hand, when the CT saturates at the end of the first cycle, the second derivative is lower than its threshold and cannot detect CT saturation, despite the low security margin of the adaptive threshold. If lower security margins are considered, the adaptive method may fail to operate correctly in the presence of noise.

4.2 Effect of burden power factor

Power factor of the CT secondary burden can affect the shape of current waveform during the distorted sections [27]. Therefore the derivative of current during the distorted sections might be changed by the burden power factor. For the previous simulated cases, power factor of the CT burden was 0.94, as the burden of a digital or a static relay is mainly resistive. For electromechanical relays, it can be generally considered that the burden has equal resistance and reactance [1]. Since variation of the burden power factor can affect the output of the proposed method, its performance for other power factors in the secondary winding is examined.

Power factors of the CT burdens were varied in the range of 0.5 to 1 throughout the simulations. Lower power factors are not feasible, even for electromechanical relays. The obtained results demonstrate that the margin between the second variance function and the specified thresholds narrows down for smaller power factors, particularly if the CT saturates before the primary current local extremum. Nevertheless, the proposed method could still detect CT saturation for all of the simulations. The burden power factor for the fault current shown in Fig. 8*a* is 0.6. The fault has occurred at $t = 200$ ms and the CT has saturated 7.2 ms later. The second variance function is depicted in Fig. 8*b*. As shown, the saturation is detected rapidly only 1.6 ms after its inception.

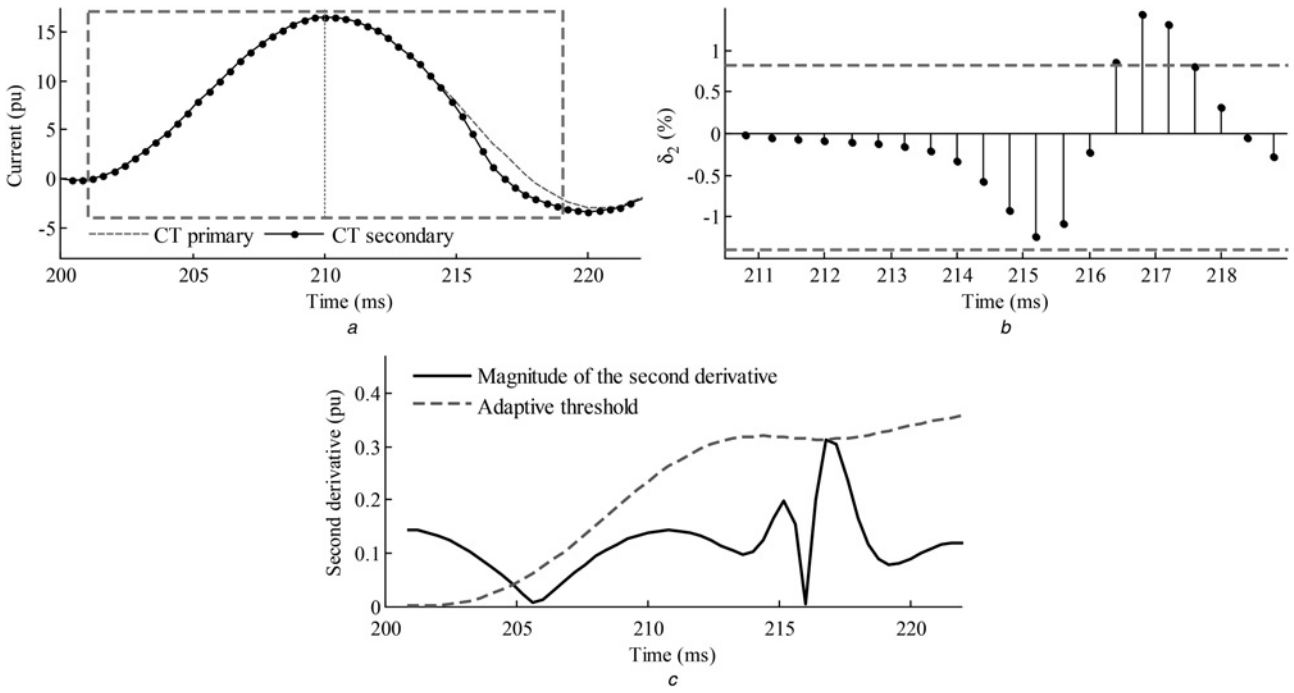

Fig. 7 *Mild CT saturation*

a CT primary and secondary currents
b Second variance function
c Performance of the adaptive CT saturation detection technique

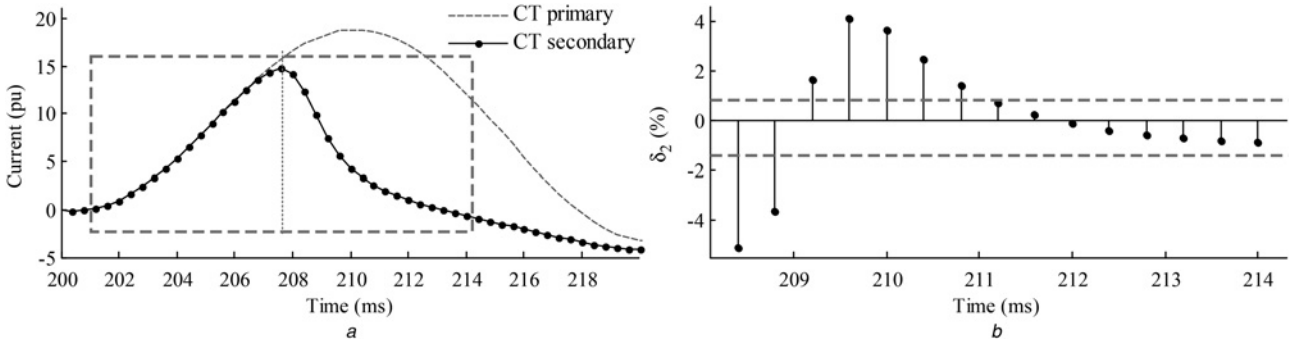

Fig. 8 *CT saturation with 0.6 lagging burden power factor*

a CT primary and secondary currents
b Second variance function

4.3 Effect of high-frequency noise

Power system fault currents are sometimes contaminated with high-frequency noise. The presence of noise in the fault current can generally increase the value of δ_2. If the CT is saturated, this increase is not a problem; it is even helpful. To test the obtained results for undistorted noisy fault currents, a wide range of possible undistorted signals were considered by changing I_d and τ of (4). Protective relays are practically equipped with low-pass analogue filters prior to the A/D converter. To correctly model the analogue process of anti-alias filtering, the initial sampling rate of the current signals is set to 1 MHz. The signal is then combined with white Gaussian noise. Afterwards, the current signals are passed through a second order Butterworth low-pass filter with 600 Hz cut-off frequency. The output of this filter is down-sampled to 2.5 kHz. Finally, the second variance function for the currents is evaluated.

Table 2 highlights some of the obtained results for two different values of signal-to-noise ratios (SNR). These results prove that performance of the proposed method remains reliable in the presence of noise. The feature that δ_2 has to be larger than its thresholds for two consecutive samples in order to detect CT saturation makes the algorithm even more robust to noise.

Noise immunity is among the advantages of the proposed method over the derivative-based methods of [14, 17]. The approach suggested in [14] is based on the third derivative of current, which is more sensitive to noise, compared to the second derivative employed in this paper. Another reason for noise immunity of this method is the large security margins considered for the thresholds of δ_2. If the

doi: 10.1049/iet-gtd.2011.0476

Table 2 Effect of noise on the second variance function

I_d	τ, ms	SNR = 25 dB		SNR = 30 dB	
		Min $\{\delta_2\}$, %	Max $\{\delta_2\}$, %	Min $\{\delta_2\}$, %	Max $\{\delta_2\}$, %
0.25	10	−0.68	0.53	−0.23	−0.01
0.25	30	−0.83	0.25	−0.26	0.10
0.25	50	−0.76	0.39	−0.29	0.17
0.25	70	−0.55	0.32	−0.39	0.15
0.25	90	−0.69	0.32	−0.32	0.19
0.50	10	−0.55	0.27	−0.46	0.06
0.50	30	−0.56	0.18	−0.38	0.10
0.50	50	−0.46	0.33	−0.28	0.04
0.50	70	−0.55	0.48	−0.26	0.27
0.50	90	−0.63	0.32	−0.09	0.29
0.75	10	−0.71	0.40	−0.63	0.12
0.75	30	−0.51	0.30	−0.39	0.17
0.75	50	−0.65	0.33	−0.32	0.16
0.75	70	−0.47	0.68	−0.29	0.26
0.75	90	−0.46	0.40	−0.19	0.20
1.00	10	−0.62	0.07	−0.42	−0.02
1.00	30	−0.67	0.17	−0.39	0.06
1.00	50	−0.58	0.51	−0.28	0.20
1.00	70	−0.38	0.40	−0.21	0.25
1.00	90	−0.35	0.52	−0.25	0.28

method of [14] uses such large security margins, it can no more detect mild CT saturations.

5 Real data tests

In order to further verify performance of the proposed algorithm, it is tested using some recorded real distorted and undistorted fault currents. Current signals flowing through a real 230/63 kV, YNd power transformer recorded at 1.6 kHz were analysed. In this event, an external phase-to-ground fault occurs on the high-voltage side of the transformer. Fig. 9*a* shows the first two cycles of phase B post-fault current on the secondary side of the CT. The sum of the three-phase currents on the secondary side of the CTs is compared with the recorded neutral current in Fig. 9*b*. The small difference between the two depicted graphs indicates that there is a relatively mild saturation in at least one of the three CTs during the first cycle. The degree of saturation increases substantially during the second cycle. The second difference functions of the first two cycles are plotted in Figs. 9*c* and *d*. The dashed horizontal lines represent the thresholds associated with the 1.6 kHz sampling rate. For both cycles, δ_2 can correctly detect CT saturation. In the first cycle, saturation is identified at the 145th sample, when δ_2 is −5.20%. For the second cycle that the degree of saturation is more severe, δ_2 increases and reaches 34.06% at the 174th sample. CTs of phases A and C are not saturated and the proposed method does not detect saturation for these phases. The maximum magnitude of δ_2 for phases A and C are 0.73 and 0.72%, respectively.

Performance of the proposed method for a fault flowing through a real 115/13 kV, 40 MVA, YNd transformer is also tested. For this case CTs of phases A and B are saturated. Table 3 displays the results obtained for the first cycle of the three-phase post-fault currents. In this table, $\delta_{2,m}$ denotes the largest magnitude of the second variance function. This table shows that δ_2 for phases A and B currents is as large as −4.18 and −8.10%, respectively; that is, the currents of these phases are distorted by CT saturation. The saturation is determined for both phases 1.25 ms after its inception. CT of phase C is not saturated and as presented in Table 3 this method has not detected any saturation for this phase. Successful performance of the proposed technique for real distorted and undistorted fault currents suggest that it can be a candidate to detect CT saturation in industrial applications.

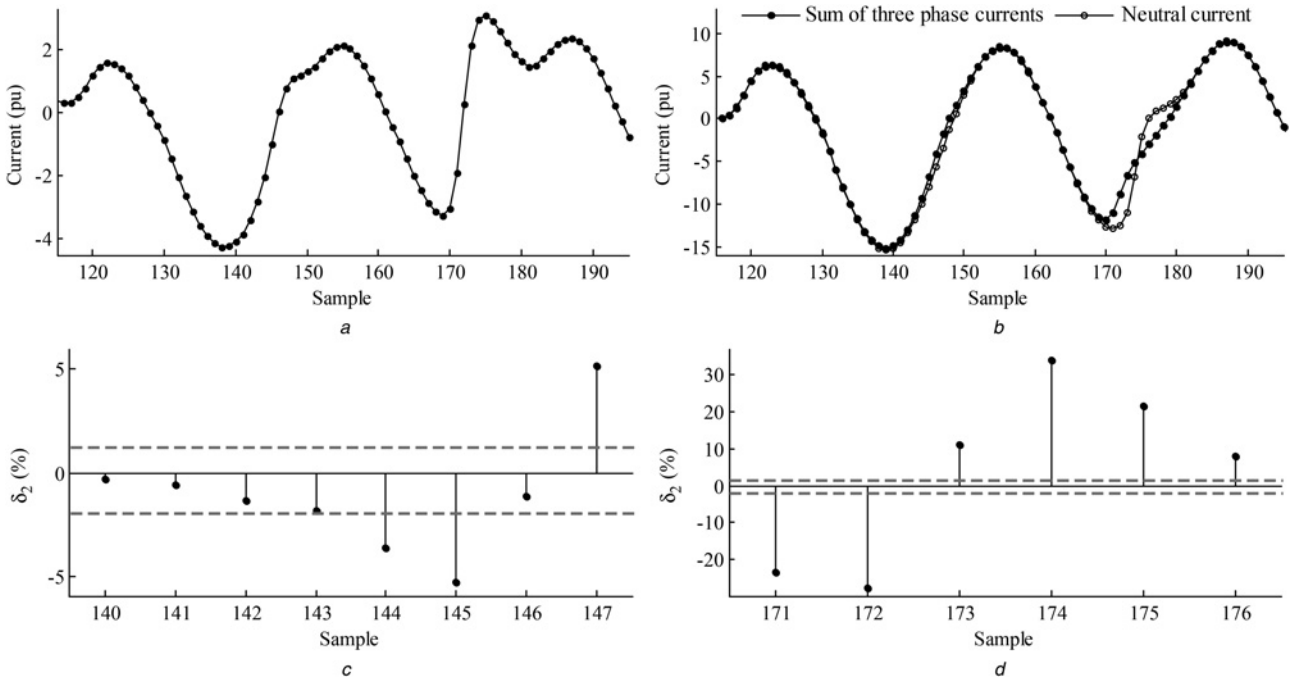

Fig. 9 *Recorded CT saturation data*

a Distorted fault current
b Sum of three-phase currents and neutral current
c δ_2 for the first post-fault cycle
d δ_2 for the second post-fault cycle

Table 3 Experimental results obtained for a 115/13 kV transformer

Phase	$\delta_{2,1}$, %	$\delta_{2,2}$, %	$\delta_{2,m}$, %	Δt_{SD}, ms
A	−3.64	−4.18	−4.18	1.25
B	−5.94	−6.50	−8.10	1.25
C	–	–	−0.47	–

6 Conclusion

By subtracting the derivatives of the symmetrically located samples at the two sides of the current local extremum, this paper defined a variance function to detect CT saturation. Based on the obtained results for undistorted fault currents, a pair of pre-set lower and upper thresholds is specified for the variance function. These thresholds are not system dependent and can be used to detect fast and mild CT saturation conditions.

Extensive simulation studies and experimental results proved that the proposed method has the following features:

1. This technique is independent of the CT characteristics, such as its remanence, magnetisation curve, burden and so on.
2. The correct performance of this method is not affected by fault current features such as decaying DC time constant and noise.
3. This method responds rapidly, and so it can prevent relay maloperation caused by CT saturation on time.
4. The accuracy of this algorithm is irrespective of the saturation inception time. Therefore it can be used to reduce the CT requirements of a relay.
5. The wide margin between the variance function and the specified thresholds during saturation conditions confirms the reliability of this method.

7 Acknowledgment

This work was supported by the University of Tehran under Grant no. 8101064-1-02.

8 References

1 Ziegler, G.: 'Numerical differential protection: principles and applications' (John Wiley & Sons, 2005, 1st edn.)
2 Applications for SIPROTEC protection relays – 400 kV overhead transmission protection, available at http://siemens.siprotec.de/download_neu/applications/SIPROTEC/english/Appl_13_400 kV_OHL_Protection_en.pdf, accessed June 2011
3 B30 Bus Differential System, UR Series Instruction Manual for 5.8x Product Version, Manual P/N: 1601-0109-V1 (GEK-113543), available at http://www.gedigitalenergy.com/products/manuals/b30/b30man-V1.pdf, accessed June 2011
4 IEEE Standard C37.235: 'IEEE guide for the application of Rogowski coils used for protective relaying purposes', 2007
5 Kojovic, L.A.: 'Rogowski coils suit relay protection and measurement', *IEEE Comput. Appl. Power Mag.*, 1997, **10**, (3), pp. 47–52
6 Villamagna, N., Crossley, P.A.: 'A CT saturation detection algorithm using symmetrical components for current differential protection', *IEEE Trans. Power Deliv.*, 2006, **21**, (1), pp. 38–45
7 Khorashadi-Zadeh, H., Sanaye-Pasand, M.: 'Correction of saturated current transformers secondary current using ANNs', *IEEE Trans. Power Deliv.*, 2006, **21**, (1), pp. 73–79
8 Lu, Z., Smith, J.S., Wu, Q.H.: 'Morphological lifting scheme for current transformer saturation detection and compensation', *IEEE Trans. Circuits Syst.*, 2008, **55**, (10), pp. 3349–3357
9 Lin, X., Zou, L., Tian, Q., Weng, H., Liu, P.: 'A series multiresolution morphological gradient-based criterion to identify CT saturation', *IEEE Trans. Power Deliv.*, 2006, **21**, (3), pp. 1169–1175
10 Li, F., Li, Y., Aggarwal, R.K.: 'Combined wavelet transform and regression technique for secondary current compensation of current transformers', *IEE Proc. Gener. Transm. Distrib.*, 2002, **149**, (4), pp. 497–503
11 Hong, Y.Y., Chang-Chian, P.C.: 'Detection and correction of distorted current transformer current using wavelet transform and artificial intelligence', *IET Gener. Transm. Distrib.*, 2008, **2**, (4), pp. 566–575
12 Yu, C.S.: 'Detection and correction of saturated current transformer measurements using decaying DC components', *IEEE Trans. Power Deliv.*, 2010, **25**, (3), pp. 1340–1347
13 Hooshyar, A., Sanaye-Pasand, M.: 'CT saturation detection based on waveform analysis using a variable-length window', *IEEE Trans. Power Deliv.*, 2011, **26**, (3), pp. 2040–2050
14 Kang, Y.C., Ok, S.H., Kang, S.H., Crossley, P.A.: 'Design and evaluation of an algorithm for detecting current transformer saturation', *IEE Proc. Gener. Transm. Distrib.*, 2004, **151**, (1), pp. 27–35
15 Nam, S.R., Park, J.Y., Kang, S.H., Kezunovic, M.: 'Phasor estimation in the presence of DC offset and CT saturation', *IEEE Trans. Power Deliv.*, 2009, **24**, (4), pp. 1842–1849
16 Kang, Y.C., Yun, J.S., Lee, B.E., Kang, S.H., Jang, S.I., Kim, Y.G.: 'Busbar differential protection in conjunction with a current transformer compensating algorithm', *IET Gener. Transm. Distrib.*, 2008, **2**, (1), pp. 100–109
17 Wiszniewski, A., Rebizant, W., Schiel, L.: 'Correction of current transformer transient performance', *IEEE Trans. Power Deliv.*, 2008, **23**, (2), pp. 624–632
18 Dashti, H., Sanaye-Pasand, M., Davarpanah, M.: 'Fast and reliable CT saturation detection using a combined method', *IEEE Trans. Power Deliv.*, 2009, **24**, (3), pp. 1037–1044
19 Technical Manual of Areva MiCOM P740 Numerical Busbar Protection, P740/EN T/D11, Available at ftp://ftp.areva-td.com/P740_EN_T_D11.pdf, accessed June 2011
20 Lyons, R.G.: 'Streamlining digital signal processing: a tricks of the trade guidebook' (John Wiley & Sons-IEEE Press, 2007, 1st edn.)
21 Pan, J., Vu, K., Hu, Y.: 'An efficient compensation algorithm for current transformer saturation effects', *IEEE Trans. Power Deliv.*, 2004, **19**, (4), pp. 1623–1628
22 Application Manual of REB500/REB500sys (Busbar Differential Relay), ABB Relay Catalogue – 1MRB 520 308-Ben, available at http://www05.abb.com/global/scot/scot313.nsf/veritydisplay/455c38fe423b2d2bc125753d005dced5/$File/1MRB520308-BEN_B_en_Numerical_Station_Protection_System_REB500-REB500sys.pdf, accessed June 2011
23 Lucas, J.R.: 'Representation of magnetisation curves over a wide region using a non-integer power series', *Int. J. Electr. Eng. Educ.*, 1988, **25**, (4), pp. 335–340
24 Annakkage, U.D., McLaren, P.G., Dirks, E., Jayasinghe, R.P., Parker, A.D.: 'A current transformer model based on the Jiles–Atherton theory of ferromagnetic hysteresis', *IEEE Trans. Power Deliv.*, 2000, **15**, (1), pp. 57–61
25 IEEE Standard C37.234: 'IEEE guide for protective relay applications to power system buses', 2009
26 Gangadharan, P.K., Sidhu, T.S., Finlayson, G.J.: 'Current transformer dimensioning for numerical protection relays', *IEEE Trans. Power Deliv.*, 2007, **22**, (1), pp. 108–115
27 Wright, A.: 'Current transformers: their transient and steady state performance' (Chapman and Hall, 1968)

9 Appendix

The simulated power system is shown in Fig. 10. The related data and parameters of this 50 Hz power system are presented in Table 4.

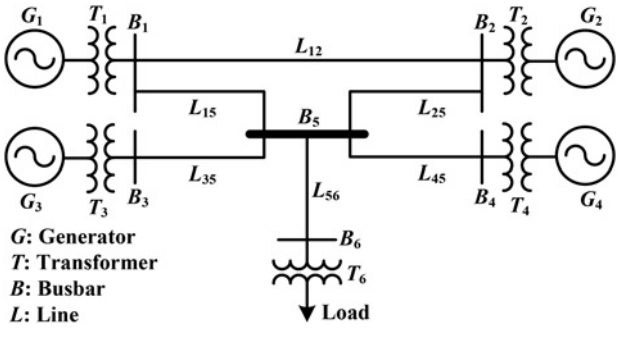

Fig. 10 *Simulated power system*

doi: 10.1049/iet-gtd.2011.0476

Table 4 Specifications of the power system components

Component	Specifications	Component	Specifications
generator 1	$V_{rated} = 15.75$ kV, $S_{rated} = 115$ MVA	Line 12	98.7 km, $Z_1 = 2.9 + j33.7\ \Omega$, $Z_0 = 27.5 + j89.6\ \Omega$
generator 2	$V_{rated} = 21$ kV, $S_{rated} = 1455$ MVA	Line 15	42.7 km, $Z_1 = 1.3 + j14.6\ \Omega$, $Z_0 = 10.7 + j43.7\ \Omega$
generator 3	$V_{rated} = 15.75$ kV, $S_{rated} = 1140$ MVA	Line 25	82.9 km, $Z_1 = 2.4 + j28.3\ \Omega$, $Z_0 = 23.5 + j77.4\ \Omega$
generator 4	$V_{rated} = 15.75$ kV, $S_{rated} = 370$ MVA	Line 35	15.8 km, $Z_1 = 0.46 + j5.4\ \Omega$, $Z_0 = 4.4 + j14.3\ \Omega$
transformer 1	$V_{rated} = 15.75/400$ kV, $S_{rated} = 115$ MVA	Line 45	35.1 km, $Z_1 = 1.0 + j12.0\ \Omega$, $Z_0 = 9.8 + j31.9\ \Omega$
transformer 2	$V_{rated} = 21/400$ kV, $S_{rated} = 1450$ MVA	Line 56	40.3 km, $Z_1 = 1.2 + j13.8\ \Omega$, $Z_0 = 11.2 + j36.6\ \Omega$
transformer 3	$V_{rated} = 15.75/400$ kV, $S_{rated} = 1190$ MVA	Load	$V_{rated} = 115$ kV, $S_{rated} = 700$ MVA, P.F.:0.95
transformer 4	$V_{rated} = 15.75/400$ kV, $S_{rated} = 370$ MVA	Transformer 6	$V_{rated} = 400/115/31.5$ kV, $S_{rated,1} = 700$ MVA